HYBRID IMPEDANCE CONTROL FOR MULTI-SEGMENTED INSPECTION ROBOT Kairo-II

C. Birkenhofer, S. Studer, J. M. Zöllner, R. Dillmann
Forschungszentrum Informatik (FZI)
Haid-und-Neu-Str. 10-14, 76131 Karlsruhe, Germany

Keywords: Hybrid Impedance Control, Multi-Segmented Robot, Force Feedback, Dynamic Modeling.

Abstract: The tremendous redundancy of the multi-segmented robot Kairo-II can be utilized to enhance general robot configuration by any inspection task. To do so, an extensive control scheme must be installed which can handle both, contact scenarios with the environment and ambiguous robot configurations. A method for implementing an appropriate scheme using Transposed Jacobians based on Hybrid Impedance Control (TJ-HIC) is described and validated for multi-segmented robots. Crucial parts of this model are identified and implemented. These are dynamic modeling of the robot in Recursive Newton-Euler equations (RNE) and a sensory system for apropriate force feedback information.

1 INTRODUCTION

Hyper-redundant systems offer great opportunity and present great challenges for control tasks. Trajectory planning, hybrid position and force control and handling redundancy require extensive control techniques. The multi-segmented robot Kairo-II is a hyper-redundant system. Its expanse, load capacity and kinematic abilities make it appropriate for inspection operations in unstructured environments.
We term the end-effector of the robot ”configurable” as different segments of the robot fulfil characteristics of the end-effector. According to serial kinematics both head- and tail-segment of Kairo-II (Figure 1) can be interpreted as end-effector of an open kinematic chain, depending on the driving direction, with head and tail segments as the robot base, respectively. The redundancy of the system furthermore can be used to position inspection segments within the kinematic chain. In this case head and tail segment represent the base of the robot. This process can be defined as an additional user-defined task. The kinematic chain of the system gets closed and gives rise to a major constraint for any control strategy arises.
Such movement offers greater opportunity for inspection tasks, but calls for complex control strategies. Deadlocks have to be detected and resolved in a appropriate way. Fundamental methods for manipulator control can be used.

The paper is organized as follows. First, the control architecture of the Kairo-II robot is presented in section 2. Crucial blocks of the control loop are here identified. Section 3 presents fundamentals of the dynamic model of the robot. This model is essential for simulating the control loop. The sensory system for

Figure 1: Multi-segmented inspection robot MAKRO-plus (similar in construction to Kairo-II). A typical robot configuration consists of 6 drive segments and 5 joint segments.

Birkenhofer C., Studer S., M. Zöllner J. and Dillmann R. (2006).
HYBRID IMPEDANCE CONTROL FOR MULTI-SEGMENTED INSPECTION ROBOT Kairo-II.
In *Proceedings of the Third International Conference on Informatics in Control, Automation and Robotics*, pages 217-222
DOI: 10.5220/0001207602170222

force detection is presented in section 4. Finally, system integration and experimental results are analyzed in detail in section 5. Summary and future work are addressed in section 6.

2 CONTROL ARCHITECTURE

2.1 Transpose Jacobian based Hybrid Impedance Control

In performing inspection tasks, a robot usually interacts with the surrounding environment. Position controlled methods can not fulfil demands of such an operation. In fact simultaneous control of position and force is necessary. Numerous basic strategies exist (Salisbury, 1980), (Hogan, 1985) and (Khatib, 1987). In the field of redundant systems those strategies have to be enhanced for two reasons:

- Ambiguity of coordinate transformations have to be handled.
- Decomposition of redundancy is usually managed by velocity controlled systems. Such systems tend to proper motion.

For these reasons, Hybrid Impedance Control, based on Transposed Jacobian (Shah and Patel, 2005) was chosen in the presented work. Main advantages of the control scheme are:

- The control algorithm is defined in the working space of the system.
- Accurate knowledge of the robot's dynamic is not necessary.
- Any higher instance for controlling the system can be integrated.

In terms of controlling a user-defined task as described in section 1 the essential requirements are fulfilled. Structure and crucial components of the control scheme are depicted in Figure 2. The control loop consists of an inner and an outer loop. While the outer loop generates desired cartesian acceleration trajectories, the inner loop controls needed motor torques directly. Redundancy of the system and possible subtasks are both handled in the inner loop.
Several blocks of the control loop have decisive character in hybrid force and motion control of the multi-segmented robot Kairo-II. Their impact on the control scheme is presented below.

2.2 Trajectory Generation

Generation of the robot's trajectory is equivalent to a transformation of a low-dimensional vector to a higher one. In taking redundancy into account a simple (low-dimensional) primary task shall be generated.
Kairo-II posesses tremendous kinematic abilities. Since this is a hyper-redundant system, tasks can be enhanced by addition of aspects (i.e. placing a sensory module) in the process of the trajectory generation. Generation of the robot's path will be processed according to the virtual line / curve algorithm (Scholl et al., 2000). This master-slave method is simple, robust and efficient. By using this method the high-dimensional input vector gets reduced to a lower dimensoinal one, as only the head-segment has to be taken into account when generating a trajectory. In contrast to other methods (i. e. (Choset and Henning, 1999)), the mechanical constraints of the robot are taken into account in the trajectory generation phase. The generated trajectory is therefor driveable for the robot.
When the environment the robot is driving becomes increasingly complex and unstructured, an adaptation towards the virtual tube algorithm (Birkenhofer et al., 2005) is desirable. Trajectory generation will then work in a higher-dimensional space. Not only the head-segment but segments essential for the additional sub-tasks are taken into account.At this stage, trajectory generation will be kept at a basic level to demonstrate the control loop's working principle.

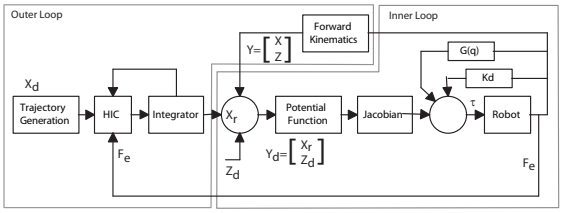

Figure 2: Transpose Jacobian based Hybrid Impedance Control, (X_d: Vector of the desired trajectory, X_r: Vector of the reference position trajectory, Z_d: Vector of the desired sub-task, Y_d: Vector of desired task requirements, F_e: contact force with the environment).

2.3 Potential Function

As part of the inner control loop, the potential function acts as a quality factor for desired movements. Aspects of optimization are taken into account to deal with the redundancy of the system. There are several criterea possible.

- Gravity keeps the components of the robot on the ground
- Minimize absolute value of all joint amplitudes
- Move inspection module to a desired position, adapt and keep the robot in a steady state.

Currently, a criterion that minimizes movements of all joints is adequate. Steady state considerations will follow.

2.4 Dynamic Modeling

The quality of dynamic modeling of Kairo-II has a large impact on the system's performance (in contrast to general TJ-HIC-applications) for two reasons:
First, good simulation of the robot is important in the early design phase of Kairo-II. (I.e. The model's accuracy has an impact on evaluating force feedback sensor system.)
Second, the use of the robot within a closed loop requires knowledge of the robot's dynamics for inverse dynamic and kinematics calculations. (I.e. Posture control of the robot has to be evaluated with regard to the robot's steady state when a user-defined additional task is processed.) The module for dynamic modelling is integrated in the work flow as depicted in Figure 3.

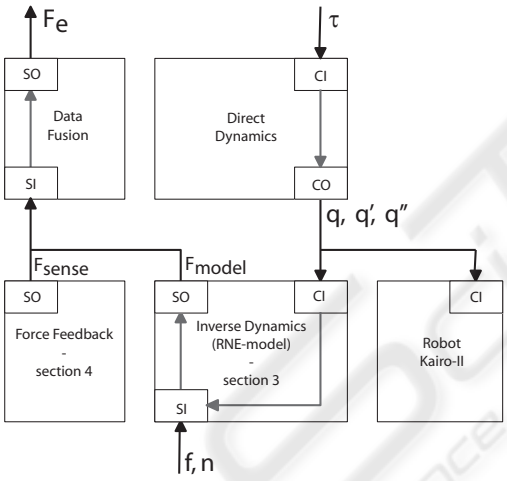

Figure 3: Work flow of the dynamic modeling and the force feedback sensor system as implemented in MCA2.3 (Scholl et al., 2001).

2.5 Force Feedback

When Kairo-II is in motion, we receive sensor values stating the current forces and moments within the robot. This is a result of the motion of the robot and its contact with the environment. At the same time, the dynamic model calculates forces and moments resulting from the sheer robot motion not considering contact with the environment. In merging sensor values with model values, we are able to calculate the external forces that act on the robot, Therefore, we assume adequate accuracy of the sensor system and the robot model. A sensor system based on strain gauge technology is therefore integrated in the module "Force Feedback" (see Figure 3).

3 DYNAMIC MODELING

For the successful implementation of the proposed control scheme it is of great importance to design an appropriate dynamic model of Kairo-II. There exist various approaches to describe the dynamics of rigid multi-body systems. Most of them face two common problems: It's hard to define the parameters and the computational complexity exceeds the capacity of a mobile system.
A modeling method that is quite efficient is the Recursive Newton-Euler equation (RNE) (Fu et al., 1987). In considering each robot link (rigid part between two joints) separately, forces and moments that apply to it can be calculated recursively. The two well-known physical laws can be used. We apply them to rotating coordinate systems:

$$\begin{aligned} F_i &= \frac{d(m_i v_i)}{dt} = m_i a_i \\ N_i &= \frac{d(I_i \omega_i)}{dt} = I_i \dot{\omega}_i + \omega_i \times (I_i \omega_i) \end{aligned} \tag{1}$$

with force F, mass m, velocity v, acceleration a, moment N, inertia I and angular velocity ω of the i-th link.
The formulation results in two sets of recursive equations: The forward equations propagate kinematics information such as angular velocity, angular acceleration and linear accelerations from the head of the robot to the tail. The backward equations propagate the forces and moments exerted on each link from the tail to the head.
To make the algorithm computationally more efficient, all values are referenced to the local coordinate system of the corresponding joints instead of computing them to the coordinate system of the head. This is demonstrated by multiplying the values with the appropriate 3×3 rotating matrices, where $\underline{R}_{i-1,i}$ transforms any vector with reference to coordinate system (x_i, y_i, z_i) to the coordinate system $(x_{i-1}, y_{i-1}, z_{i-1})$.
Inputs of the model are the current joint positions q_i, joint velocities $\dot{q}_i$ and joint accelerations $\ddot{q}_i$, while $\underline{R}_{n,0}\underline{f}_{n+1}$ and $\underline{R}_{n,0}\underline{n}_{n+1}$ are the forces and moments exerted by link n upon the environment.

$$\left\{ \begin{array}{l} q_i \\ \dot{q}_i \\ \ddot{q}_i \\ \underline{R}_{n,0}\underline{f}_{n+1} \\ \underline{R}_{n,0}\underline{n}_{n+1} \end{array} \right\} \overset{RNE}{\Longrightarrow} \left\{ \begin{array}{l} \underline{R}_{i,0}\underline{F}_i \\ \underline{R}_{i,0}\underline{N}_i \\ \underline{R}_{i,0}\underline{f}_i \\ \underline{R}_{i,0}\underline{n}_i \\ \tau_i \end{array} \right\} \tag{2}$$

(With $i = 1 \ldots n$). The model outputs the total external force $\underline{R}_{i,0}\underline{F}_i$ and moment $\underline{R}_{i,0}\underline{N}_i$ exerted on link

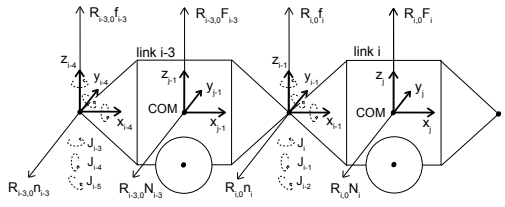

Figure 4: Simplified dynamic model of Kairo-II.

i at the center of mass (COM) for the links $i = 1 \ldots n$. Furthermore it returns the forces $\underline{R}_{i,0}\underline{f}_i$ and moments $\underline{R}_{i,0}\underline{n}_i$ exerted on link i by link $i-1$ at the position of joint i and the input force/torque τ_i for joint i.
Each link is specified by a set of 14 parameters, which describe the kinematics of the link, its mass and its inertia. So, to describe the robot Kairo-II in its standard configuration with 6 segments and 15 joints, more than 200 parameters would have to be defined. Furthermore, the values of inertia have to be determined for each of them.

3.1 Simplified Dynamic Modeling

To avoid the problem of complexity, a simplified model of the robot is presented. As two segments of Kairo-II are linked by three joints, we would have to define $3 \cdot 14 = 42$ parameters. We replace the three real joints by three virtual joints (J_i, J_{i-1}, J_{i-2}), that are centred at one point just in between two segments (see Figure 4). The joint's coordinate systems have the same origin, and their axes of rotation form an orthogonal coordinate system.
In this way the links $i-1$ and $i-2$ are zero-links with mass, inertia and displacement vectors all being zero. As a result the number of parameters to determine decreases from 42 to 20.
This also reduces the enormous number of output values of our model. With the reduced model all output forces/moments are located either at the center of mass of the segments or at the location of the virtual joints which simplifies the interpretation of the values and the integration into the control scheme.

4 SENSOR SYSTEM

The TJ-HIC control scheme needs information about forces and moments arising within the real robot. By fusing this sensor information with data from the dynamic model, differential data can be obtained. $F_e = F_{model} - F_{sense}$. With F_e as differential force after the robot's contact with the environment. In minimizing F_e a movement close to the desired movement generated by the trajectory planner is achieved.
In installing a sensor system for force feedback, major effort has to be put into the sensor's position. According to Figure 4 the sensor's coordinate systems should match to the dynamic modeling systems. Therefore, a sensor system is presented that is able to detect forces and moments in the model's coordinate systems.
Three sensor applications fulfil these requirements. They provide information on arising forces and moments along the axes of the dynamic model or can be at least transformed easily.

Rotation around x-axis Implicit torque measurement within rotational gears

Forces along y-, z-axis Explicit torque measurement within mechanic components (flange plate)

Forces along x-axis Explicit torque measurement by analyzing drive segment motor currents

The biggest impact on constraint motion is provided by explicit torque measurement along y- and z-axis. As a result of this, sensory feedback virtual tube can be adapted to minimize torsions that affect the manipulator. Gathering this sensory information is described in the next sections. Measuring torques and forces along the x-axis is not covered in this paper.

4.1 Architecture

For a typical robot configuration of 6 drive segments and 5 joint segments and well-known masses of the components, a detection of arising torques of about $25\ Nm$ to $200\ Nm$ is desirable to be detected. By making this information available, adaptation of the virtual tube is possible. The linear structure of the robot, minding the law of the levers, prefers torques to forces for analysis. Torques in direction of y- and z-axes are to be measured. Any combination of those vectors is valid.
Analyses in (Birkenhofer et al., 2004) have proven that force and torque primarily affect the flange plate. Deformations resulting of affecting forces are here to be measured best. The presented sensor system meets requested accuracy. It is based on strain gauge technology.
To detect the direction of affecting moments non-ambiguously, a sensor array is necessary. Three pairs of sensors with an angular distance of 60 degree are installed. Therefore, six pairs of strain gauges are applied. Opposing strain-gauges in each case make up a full measuring bridge, providing optimal temperature compensation. The positions of the single sensors are named $w_{1+/-}, w_{2+/-}, w_{3+/-}$. Thereby, three sensor signals are derived: $w_{1..3}$.
According to the general strain-gauges equation

$$\frac{\Delta R}{R_0} = \frac{\Delta U}{U_0} = k.\frac{\Delta l}{l_0} \qquad (3)$$

maximal sensor resolution (i.e. minimal detectable elongation δl) can be achieved by optimizing three sets of parameters:

- Enhancing circuits voltage U respectively resistance R.
- Scaling down factor k, which is subject to material properties.
- Minimizing SNR of the sensors circuitry.

While items 1 and 2 underlie mechanical constraints, major work has been put into SNR reduction of the electrical circuitry, sensor's cabling and sensor's fixing. As a result an amplification factor of $k = 5826$ results in a signal's amplitude of about 4000 LBS (with noise in a range of 500 LSB).

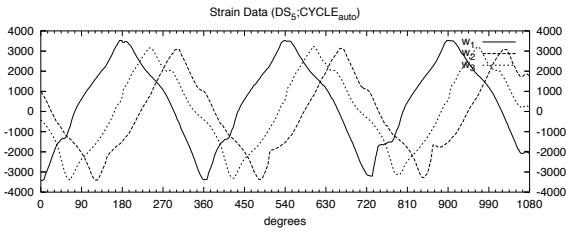

Figure 5: A constant load that is rotating around the flange plate causes alternating amplitutes of sensor signals $w_{1..3}$. (x-axis: angle in deg, y-axis: sensor value in LSB).

As seen in Figure 5 angular detection of applying forces are possible. The sensor meets the control scheme's demands.

4.2 Signal Optimization

Three primary factors affect sensory accuracy and therefore reduce measurement reading interpretation respectively:

Hysteresis Measured magnitude is at a maximum of about $\pm 1\ \mu m/m$ strain

Long-term drift is in a range of about $\pm 1.25\ \mu m/m$ strain

Temperature compensation's residual error is compensated by a linear approach. An auto-fit algorithm is used, to minimize the error signal q_i.

$$q_i = \left\{ w_i(j) - \Big[o_i + p_i \cdot T(j) \Big]; \forall j \right\} \quad (4)$$

With j as a single tuple in the data series, $w_i(j)$ as current strain value and $T(j)$ as the according temperature. The algorithm optimizes q_i by minimizing the least square error $e(p_i, o_i)$ iteratively. The algorithm will be aborted after five iterations, as the auto-fitting process results then in a remaining residual error in a range of ± 50 counted measurands for the falling branch of temperature. This equals to $\pm 0.25\ \mu m/m$, which is close to the desired sensor resolution.

In order to apply torques to the flange plate's deformation, the direct sensor model maps three sensor signals $[w_1, w_2, w_3]$ to moments $[M_y, M_z]$ according to axes y,z of the flange plate coordinate system. A calibration will determine a set of model parameters C for a provided set of calibration data, comprising l data tuples $[M_y, M_z, w_1, w_2, w_3]^\lambda;\ 1 \leq \lambda \leq l$.
Therefore, we need some approximation with coefficients $c_{ij} \in C$:

$$M_y^\lambda \approx c_{1,0} + c_{1,1} w_1^\lambda + c_{1,2} w_2^\lambda + .. + c_{1,7} w_1^\lambda w_1^\lambda \ .. \quad (5)$$

$$M_z^\lambda \approx c_{2,0} + c_{2,1} w_1^\lambda + c_{2,2} w_2^\lambda + .. + c_{2,7} w_1^\lambda w_1^\lambda \ .. \quad (6)$$

As this is an over-determined, linear equation system, least squares method provides optimal solution by querying all calibration data tuples for either M_y^λ or M_z^λ. The vector of variables can be created in different ways. In this work, the expressions (7) and (8) render best results.

$$W_{lin}^\lambda = [\ 1\ w_1^\lambda\ w_2^\lambda\ w_3^\lambda\ ] \quad (7)$$

$$W_{poly^3}^\lambda = [\ 1\ w_1^\lambda\ w_2^\lambda\ w_3^\lambda\ (w_1^\lambda)^2\ (w_2^\lambda)^2\ (w_3^\lambda)^2 ... \\ ...(w_1^\lambda)^3\ (w_2^\lambda)^3\ (w_3^\lambda)^3\ ] \quad (8)$$

W_{lin}^λ is simple and stable, $W_{poly^3}^\lambda$ is better suited to cope with deformations or harmonics at the inflection points of the strain signals. Vectors which include cross product terms (as $w_1^\lambda \cdot w_2^\lambda$) do not respond in an adequate way.

5 INTEGRATION & RESULTS

In this paper the TJ-HIC control scheme was presented and identified as adequate for an implementation in the multi-segmented inspection robot Kairo-II. Two major function blocks of this scheme were presented in detail: dynamic modeling and the force feedback sensor. Outputs of both are to be fused in a further function block to close the control loop.

5.1 Sensor System

Some optimization criteria have been presented to deal with the sensor's accuracy. As a result we get an angular and amplitude decomposition of the signal which is presented in table 1. The presented results indicate a good angular resolution (Birkenhofer et al.,

Table 1: Angular and amplitude decomposition.

	$25\ Nm$	$200\ Nm$
angular error	$\pm 19°$	$\pm 12,8°$
amplitude error	$\pm 26\%$	$\pm 18,3\%$

2005). Amplitude resolution can be optimized by complex material analyses. As we use the signal for impedance control, the signal's quality can be weighted by impedance control factors M_d, B_d and K_d. A focus on the angular resolution signal is therefore possible. With this method influence of the amplitude of the signal can be minimized, whereas the angular value of the signal gets strengthened.

5.2 Dynamic Modeling

The dynamic modeling of Kairo-II has been realized as functional block in the software framework MCA. Appropriate coordinate systems have been identified to handle both efficient calculations within the model and simple sensor fusion with other modules. Therefore, a simplified dynamic modeling was introduced that meets the mechanical requirements and reduces the number of parameters drastically.
Sensor fusion can be implemented in a new module easily, as all data sources (dynamic modeling, sensor system) provide data in similar coordinate systems.
The following example depicts the working principle of the algorithm (see Figure 6). All robot joints are positioned in their nullposition. The robot is fixed at its left end. In applying joint velocities (ALPHA_M_qd) $3\frac{1}{s}$ and joint accelerations (ALPHA_M_qdd) $3\frac{1}{s^2}$ to all joints. Forces and moments within the system arise. They can be calculated according to the RNE algorithm. Results are presented in table 2 and depicted as vectors in Figure 6.

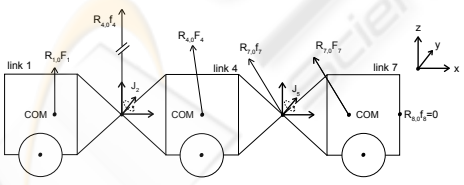

Figure 6: Robot configuration with three segments.

Table 2: Sensor Outputs of the RNE algorithm (forces [N], moments [Nm]).

i	1	4	7
$\underline{R}_{i,0}\underline{F}_i$	$\begin{pmatrix} 0 \\ 0 \\ 67.17 \end{pmatrix}$	$\begin{pmatrix} -14.19 \\ 0 \\ 99.47 \end{pmatrix}$	$\begin{pmatrix} -50.06 \\ 0 \\ 82.85 \end{pmatrix}$
$\underline{R}_{i,0}\underline{f}_i$	$\begin{pmatrix} -64.25 \\ 0 \\ 249.49 \end{pmatrix}$	$\begin{pmatrix} -64.25 \\ 0 \\ 182.31 \end{pmatrix}$	$\begin{pmatrix} -50.06 \\ 0 \\ 82.85 \end{pmatrix}$
$\underline{R}_{i,0}\underline{N}_i$	$\begin{pmatrix} 0 \\ 0 \\ 0 \end{pmatrix}$	$\begin{pmatrix} 0 \\ -0.41 \\ 0 \end{pmatrix}$	$\begin{pmatrix} 0 \\ -0.34 \\ 0 \end{pmatrix}$
$\underline{R}_{i,0}\underline{n}_i$	$\begin{pmatrix} 0 \\ -106.28 \\ 0 \end{pmatrix}$	$\begin{pmatrix} 0 \\ -54.71 \\ 0 \end{pmatrix}$	$\begin{pmatrix} 0 \\ -10.29 \\ 0 \end{pmatrix}$

6 CONCLUSION

A control scheme for multi-segmented robots was presented. As controlling the robot's redundancy is both challenging and promising, this scheme can handle the ambiguity of the system. Crucial modules of the TJ-HIC scheme were identified and implemented in this paper. As the other - relevant - modules of the control scheme (i.e. trajectory planning and potential function) are kept to minimal complexity, the control loop can be closed now.
Future work has to be done in the field of not only handling but using the redundancy of Kairo-II. In doing so, huge driving capabilities are expected. The system is then able not only to fulfill a main task but also an user-defined subtask like positioning an inspection module or avoiding obstacles.

REFERENCES

Birkenhofer, C., Hoffmeister, M., Zöllner, J.-M., and Dillmann, R. (2005). Compliant motion of a multi-segmented inspection robot. In *IRS*, Edmonton.

Birkenhofer, C., Scholl, K.-U., Zöllner, J.-M., and Dillmann, R. (2004). A new modular concept for a multi-joint, autonomous inspection robot. In *(IAS 8)*.

Choset, H. and Henning, W. (1999). A follow-the-leader approach to serpentine robot motion planning. *SCE Journal of Aerospace Engineering*.

Fu, K., Gonzalez, R. C., and Lee, C. G. (1987). *Robotics - Control, Sensing, Viion and Intelligence*. McGraw-Hill International Editions.

Hogan, N. (1985). Impedance control: An approach to manipulation, parts i - iii. *ASME J. Dynam. Syst., Meas., Contr.*, 107:1–24.

Khatib, O. (1987). A unified approach to motion and force control of robot manipulators: The operational space formulation. *IEEE Journal on Robotics and Automation*, 3(1):43–53.

Salisbury, K. (1980). Acitve stiffness control of manipulators in cartesian coordinates. *IEEE Int. Conf. Robotics and Automation*, pages 95–100.

Scholl, K.-U., Albiez, J., and Gassmann, B. (2001). Mca - an expandable modular controller architecture. In *3rd Real-Time Linux Workshop*.

Scholl, K.-U., Kepplin, V., Berns, K., and Dillmann, R. (2000). Controlling a Multi-joint Robot for Autonomous Sewer Inspection. In *ICRA*.

Shah, M. and Patel, R. (2005). Transpose jacobian based hybrid impedance control of redundant manipulators. In *CCA*, pages 1367– 1372.